Biomedicine & Pharmacotherapy 192 (2025) 118621

Contents lists available at ScienceDirect

Biomedicine & Pharmacotherapy

journal homepage: www.elsevier.com/locate/biopha

Modelling-filtered drug repurposing and first-in-protein SPR validation of histone deacetylase 4 inhibitors for Ataxia-telangiectasia

Alessia Distefano [a], Matteo Pappalardo [b], Roberta Turco [b,1], Giuseppe Grasso [a,*], Salvatore Guccione [b]

[a] Department of Chemical Sciences, University of Catania, v.le A. Doria 6, Catania 95125, Italy
[b] Department of Drug and Health Sciences, University of Catania, v.le A. Doria 6, Catania 95125, Italy

ARTICLE INFO

Keywords:
HDAC4
Surface Plasmon Resonance
Asenapine
Drug repurposing

ABSTRACT

Ataxia-telangiectasia is a neurodegenerative disorder characterised by ATM deficiency and aberrant nuclear accumulation of Histone deacetylase 4 (HDAC4) in Purkinje neurons. Targeting HDAC4 has thus emerged as a promising therapeutic strategy. Here, we employed a drug-repositioning approach to identify new HDAC4 modulators from an EMA-approved compound library. *In silico* screening selected asenapine, a second-generation antipsychotic, through consensus scoring across four independent docking functions and low predicted binding free energy (ΔG), positioning it among the most thermodynamically stable candidates. Surface plasmon resonance analysis confirmed high-affinity binding to immobilised HDAC4, enabling extraction of kinetic and thermodynamic parameters that characterise the allosteric mechanism underlying HDAC4–asenapine complex formation. Competitive assay with tasquinimod, a known HDAC4 modulator, revealed that asenapine exhibits higher affinity supporting its candidacy for further pharmacological development. These findings underscore the utility of combining repositioning pipelines with real-time affinity quantification to accelerate the discovery of selective HDAC4-targeted therapeutics for Ataxia–Telangiectasia.

1. Introduction

Ataxia-telangiectasia (A-T) is a devastating, multisystem autosomal recessive disorder marked by progressive cerebellar ataxia, oculocutaneous telangiectasias, immunodeficiency, and a pronounced predisposition to lymphoid malignancies. With an incidence of approximately 1 in 40,000–100,000 live births and no curative intervention available, affected patients typically succumb to pulmonary complications or cancer in early adulthood [1,2]. The underlying genetic lesion—biallelic loss-of-function mutations in the ATM gene—abrogates a central serine/threonine kinase that orchestrates DNA double-strand break repair, cell-cycle checkpoints, and apoptotic signalling via substrates such as p53, Chk2, and H2AX [3,4]. Seminal work by Li et al. uncovered that ATM deficiency drives aberrant nuclear retention of histone deacetylase 4 (HDAC4) in cerebellar Purkinje neurons, causing histone H3 hypoacetylation, down-regulation of neuroprotective transcripts, and eventual apoptosis [2,5,6]. As a class IIa HDAC, HDAC4 exhibits low intrinsic catalytic turnover yet exerts profound regulatory effects through signal-dependent nucleo-cytoplasmic shuttling and a regulatory zinc-binding domain adjacent to its catalytic core [7,8]. HDAC4 comprises an N-terminal regulatory domain, which interacts with transcription factors, and a C-terminal zinc-dependent catalytic domain, critical for substrate recognition and complex formation with HDAC3–NCoR. Structural data reveal an intermolecular disulphide bond between Cys669 and Cys700 of adjacent monomers, suggesting redox-sensitive stabilisation of the functional assembly [9]. Pharmacological inhibition of HDAC4 thus emerges as an attractive strategy to restore epigenetic homeostasis and impede neurodegeneration in A-T [10]. Drug repositioning accelerates therapeutic discovery by harnessing existing safety, efficacy, and pharmacokinetic data of approved agents [11–13].

The European Medicines Agency's Orphan Medicinal Products Designation program curates a library of over 1000 approved compounds with orphan designation, offering a rich source for HDAC4 inhibitor candidates [14]. In our study, this EMA-approved repository was screened *in silico* using advanced molecular-modelling pipelines

* Corresponding author.
E-mail address: grassog@unict.it (G. Grasso).
[1] Master's degree thesis in Pharmaceutical Chemistry and Technology, Department of Drug and Health Sciences, University of Catania

https://doi.org/10.1016/j.biopha.2025.118621
Received 19 August 2025; Received in revised form 25 September 2025; Accepted 1 October 2025
Available online 3 October 2025
0753-3322/© 2025 The Authors. Published by Elsevier Masson SAS. This is an open access article under the CC BY-NC-ND license (http://creativecommons.org/licenses/by-nc-nd/4.0/).

integrating docking, pharmacophore mapping, and dynamic ensemble refinement to pinpoint high-affinity ligands. To our knowledge, this work represents the first application of an optimized Surface Plasmon Resonance (SPR) protocol to directly interrogate the binding of protein macromolecules with small organic compounds, in the context of drug repositioning. Through the exploitation of non-covalent interactions between HDAC4 enzyme, immobilised on a suitably functionalized sensor surface, and the drugs under investigation, SPR enables the quantitative assessment of binding affinities, conformational dynamics, and allosteric modulation with micromolar sensitivity [15,16]. SPR enables the direct extraction of kinetic and equilibrium constants, which are fundamental to describing the molecular mechanism of interaction [17,18]. These parameters provide a robust *in vitro* validation framework for drug candidates initially identified through in silico screening.

Among the various candidates screened through molecular modelling, the antipsychotic drug asenapine emerged as the most promising. Asenapine is a second-generation antipsychotic approved for the treatment of schizophrenia and acute manic or mixed episodes in bipolar I disorder. It works primarily by blocking serotonin (5-HT_2A) and dopamine (D_2) receptors, helping to rebalance neurotransmitter activity in the brain [19]. Although asenapine is clinically approved for psychiatric indications, its tetracyclic, protonable, and aromatic structure [23] renders it a compelling candidate for drug repurposing. This structural suitability, combined with consistent top-ranking across four independent scoring functions and a correct orientation within the HDAC4 catalytic site, provided a strong rationale for its experimental evaluation as a potential HDAC4 modulator. In particular, its predicted binding free energy (ΔG binding) placed it within the most thermodynamically stable group of compounds analysed, thus identifying it as the most suitable candidate for subsequent experimental validation.

As a pharmacological benchmark, tasquinimod, a quinoline-3-carboxamide derivative with submicromolar HDAC4 modulatory activity, was included to contextualise our repositioned leads SPR profiles [20–22].

By juxtaposing SPR-derived binding parameters of tasquinimod with asenapine, we delineated compounds exhibiting equal or superior affinities and distinct allosteric footprints, thereby prioritizing candidates for downstream scaffold hopping [23], cellular and *in vivo* evaluation. This integrative pipeline melding drug repositioning, state-of-the-art molecular modelling, and pioneering SPR biophysics, charts a rapid, de-risked route to novel HDAC4 inhibitors with translational potential for A-T and related neurodegenerative disorders.

2. Material e methods

2.1. Ligand database preparation

A curated library of 4642 FDA and EMA approved drugs was obtained from the drug central 2021 [21]. Ligands were imported in SDF format and pre-processed using Flare™ v10.0.1 (Cresset®, Litlington, Cambridgeshire, UK; https://www.cresset-group.com/flare/) Protonation states were assigned at pH 7.4, and 3D geometries optimized using the XED force field [24–26].

2.2. Protein preparation

The X-ray crystal structure of HDAC4 (PDB ID: 2VQM) was retrieved from the Protein Data Bank. Protein structure preparation was carried out in Flare™ v10.0.1 and Hermes (CCDC). All water molecules and ligands were removed, hydrogen atoms added, and residues protonated according to physiological pH. The binding site was defined based on the catalytic zinc-coordination sphere with a radius of 10 Å.

2.3. Virtual screening with flare

In Flare™ v10.0.1, flexible ligand docking into a rigid protein model was performed using the built-in XED-based docking algorithm [24–26]. Scoring was based on a consensus between FieldScore, ShapeScore, and XEDScore, and the top 100 ligands were retained based on combined performance across these metrics.

2.4. Virtual screening with GOLD

Parallel docking was carried out using GOLD v2025.1(https://www.ccdc.cam.ac.uk/solutions/software/gold/). GOLD is a high accuracy protein–ligand docking software based on a genetic algorithm, to predict ligand binding and flexibility [27]. The same prepared HDAC4 model was used. Ligands were docked with 10 runs per molecule and a 10 Å radius around the active site zinc ion. The defined residues were treated as flexible, and their side chains were rotated in 10° increments and scanned over 360°. Three docking scoring functions were used, namely *i)* CHEMPLP fitness, which is an empirical fitness function optimized for pose prediction; *ii)* ChemScore fitness function, which takes into account the hydrophobic-hydrophobic contact area, hydrogen bonding and ligand flexibility, by incorporating ΔG°, protein-ligand atom clash term, and an internal energy term; *iii)* GoldScore fitness function which is the original scoring function provided with GOLD. GoldScore is well suited for the prediction of ligand binding positions and takes into account factors such as H-bonding energy, van der Waals energy, metal interaction and ligand torsion strain. The scoring functions were used with default parameters. For each of the 10 GA runs, a number of 100.000 GA operations were performed on a set of five groups with a population size of 100 individuals; crossover, mutation, and migration were set to 95, 95, and 10, respectively; default cut off values of 2.5 Å for hydrogen bonds and 4.0 Å for van der Waals distance. The top 100 ligands were selected based on consensus across at least three scoring functions.

2.5. Consensus selection and ranking

Docking results from Flare™ 10.0.1 [24–26] and GOLD v2025.1 [27] were compared by evaluating overlap among the top 100 poses. Ligands that consistently ranked highly in both pipelines were prioritized. From this comparative analysis, six compounds were identified as consensus hits, exhibiting high scores and favourable binding modes in both software environments. Among these, the 9 top-ranked compounds were selected for MM/GBSA rescoring.

2.5.1. MM/GBSA rescoring

The best-ranked compound from the consensus set underwent post-docking binding energy estimation using MM/GBSA as implemented in Flare™ v10.0.1 The binding free energy (ΔG_{bind}) was calculated as:

$$\Delta G_{bind} = \quad E_{complex} - \left(E_{protein} + \quad E_{ligand}\right)$$

Energy terms included molecular mechanics (MM) using the XED force field, solvation energy via the Generalized Born (GB) model, and a non-polar surface area component [28]. Only the single best pose from the top hit was analysed to refine ranking and estimate interaction strength with HDAC4.

2.6. Surface plasmon resonance (SPR) binding analysis

2.6.1. HDAC4 immobilization on a MAR-sensor chip via amine coupling

For the immobilisation of HDAC4, a MAR sensor chip (Sartorius, Germany) was used on the Octet® SF3 surface plasmon resonance system (Sartorius, Germany). This chip is functionalized with a three-dimensional carboxymethylated dextran matrix, which affords a significantly higher immobilization capacity than the conventional CDL chip.

This is because it provides a number of reactive COOH groups on the surface that is approximately threefold greater than that of a standard CDL chip for an equivalent dextran coverage.

Prior to immobilisation, the HDAC4 stock solution, originally in Tris-HCl buffer (pH 8.0), was subjected to buffer exchange using a VIVA-SPIN® 500 centrifugal concentrator, replacing the Tris buffer with 10 mM sodium acetate (pH 4.6), which is optimal for amine coupling. In accordance with standard SPR immobilisation protocols, a pre-concentration buffer at pH 4.6 was employed. This pH offset, at least 0.5–1 unit below the estimated isoelectric point of HDAC4, facilitates optimal electrostatic attraction and ligand retention on the sensor surface. The chosen pH remains within the recommended 4–6 range typically used for amine-coupling of proteins with similar pI values [29]. The buffer exchange is necessary because the Tris buffer and its pH are incompatible with successful amine coupling. Tris contains free amino groups that, being more abundant than those on the enzyme, can react with the sensor surface in place of HDAC4. Additionally, efficient immobilization requires the pH to be below the enzyme isoelectric point (pI 6.96 for HDAC4 [30]) but above the pKa of the carboxyl groups in the carboxymethyl dextran matrix. Under these conditions, the matrix is negatively charged while the amino groups of the enzyme carry a positive charge, promoting the electrostatic attraction that drives covalent bond formation [29]. Performing the buffer exchange before sample preparation therefore eliminates both issues and optimizes enzyme immobilization.

The immobilisation procedure was performed in three sequential steps (Figure S1). First, the carboxyl groups on both CH1 (active channel) and CH2 (reference channel) were activated by injecting a freshly prepared 1:1 mixture of 0.4 M 1-ethyl-3-(3-dimethylaminopropyl) carbodiimide (EDC) and 0.1 M N-hydroxysuccinimide (NHS) at a constant flow rate of 10 μL/min for 7 min. The running buffer used during the procedure was 10 mM phosphate-buffered saline (PBS), supplemented with 20 μM $ZnCl_2$ and 0.05 % Tween 20. Immediately after activation, 135 μL of HDAC4 in acetate buffer was injected over CH1 at 10 μL/min for 7 min to allow covalent coupling. Finally, to quench remaining reactive esters and prevent nonspecific adsorption, a 1 M ethanolamine solution (pH 8.5) was injected over both channels at 10 μL/min for 420 s, followed by a 60-sec dissociation phase.

The immobilisation efficiency of HDAC4 on the MAR sensor chip was evaluated in terms of surface density, yielding an average response of 4943 RU. According to Sartorius technical documentation, the SF3 instrument reports a response where 1 RU corresponds approximately to 1 pg/mm^2 of immobilised protein. This relationship is consistent with general literature estimates, including those reported by Schasfoort [31], which associate 1 ng/mm^2 of protein with ~1000 RU using 670 nm light. Assuming a molecular weight of 132 kDa for full-length HDAC4, this value translates to an estimated surface density of $\sim 2.24 \times 10^{1}$ ° molecules per mm^2.

2.6.2. HDAC4 – drugs binding assay

Tasquinimod was dissolved in water at a final concentration of 40 mM, using 1.5 equivalents of NaOH. Serial dilutions of tasquinimod (6.25 μM, 3.13 μM, 1.56 μM, 781 nM, and 391 nM) were injected over both flow channels (CH1 and CH2) for 180 s at a constant flow rate of 30 μL/min, followed by a dissociation phase of 180 s. The running buffer contained 1 mM dithiothreitol (DTT) to maintain the cysteine residues in HDAC4 zinc-binding domain in a reduced state. After each injection, the sensor surface was regenerated by passing running buffer free of DTT for 30 s at the same flow rate.

The interaction between HDAC4 and asenapine was assessed by injecting serial dilutions of asenapine (12.5 μM, 1.56 μM, 791 nM, 391 nM, and 195 nM) over both channels under identical conditions (injection phase: 180 s; dissociation: 180 s; flow rate: 30 μL/min). The asenapine maleate stock solution was prepared in water due to its aqueous solubility. Regeneration of the sensor surface was performed after each injection using running buffer without DTT for 30 s. All measurements were performed in triplicate. Sensorgrams were processed by double-referencing, subtracting both the signal from the reference channel (CH2) and the averaged response from blank injections of running buffer.

To evaluate the effect of tasquinimod on the binding of asenapine to HDAC4, a competitive SPR assay was performed.

Specifically, two independent experiments were conducted. Firstly, increasing concentrations of asenapine (6.25 μM, 3.13 μM, 1.56 μM, 391 nM, and 195 nM) were pre-incubated with a low concentration of tasquinimod (500 nM). In the second experiment, a higher concentration of tasquinimod (5 μM) was incubated with increasing concentrations of asenapine (12.5 μM, 6.25 μM, 1.56 μM, 781 nM, and 195 nM). This was followed by a dissociation phase using the running buffer (excluding DTT) as the dissociation agent.

Each measurement was conducted in triplicate. All sensorgrams were double-referenced by subtracting both the signal from the reference channel (CH2) and the mean response from blank injections of running buffer.

3. Results and discussion

3.1. Modelling

At the end of the virtual screening process, the 10 most promising ligands were selected by comparing the top 100 molecules according to three scoring functions from Flare™ v.10.0.1 [24–26]and one from GOLD v2025.1 [27] Only ligands that appeared in at least three of these scoring functions were retained. In our case, ligands 28 and 205 were identified across all scoring functions. Fig. 1 displays all nine selected compounds, including tasquinimod. The following table reports the number of times each ligand was found to be repeated among the selected top hits.

Subsequently, we analysed the interactions of each individual ligand, considering hydrophobic interactions, hydrogen bonds, possible halogen bonds, aromatic stacking interactions, cation–π interactions, and steric hindrance. By examining the interaction maps of each ligand, we identified and reported the amino acids interacting with the target, highlighting those residues that were shared across multiple ligands (Table 2).

From Table 2, we observe that ligands 14, 110, 156, 160, and 217 interact with amino acids located in the same binding region. In contrast, ligands 205 and 43, despite obtaining good scores, bind to a region adjacent to the active site and should therefore be excluded from further in-depth studies.

Table 3 reports the predicted binding free energy (ΔG binding) of the best pose, calculated using the MM/GBSA method in Flare™ v.10.0.1 [24–26]. The results indicate that the most stable complexes are formed by ligands 14 and 156.

Comparing the data from Table 1, ligand 205 appears most frequently across the different scoring functions (4 times). However, the predicted binding energy of the HDAC4/205 complex is approximately 10 % lower than that of the corresponding complex with ligand 14 and seems to bind outside the correct binding site. A similar consideration applies to ligand 28, with the exception that it does bind within the correct site. Therefore, in terms of complex stability, ligands 14 and 156 appear to be the most favourable candidates; however, ligand 28 is the only one consistently ranked by all scoring functions.

This consistent ranking highlights asenapine as a reliable lead candidate, showing strong agreement across different scoring methods. Although its predicted binding free energy (−200.97 kcal/mol) was approximately 9 % less favourable than that of ligand 14 (−220.98 kcal/mol), asenapine uniquely occupied the correct binding site. By contrast, ligand 205, despite matching the ranking frequency of asenapine, was oriented toward a peripheral, non-functional region.

Structural comparison of the docking poses of asenapine and tasquinimod within the catalytic pocket of HDAC4 reveals marked differences in binding orientation, interaction profiles, and predicted affinity. Despite its relatively small molecular size, asenapine, as reported in Fig. 2, inserts deeply into the catalytic cavity, establishing selective and

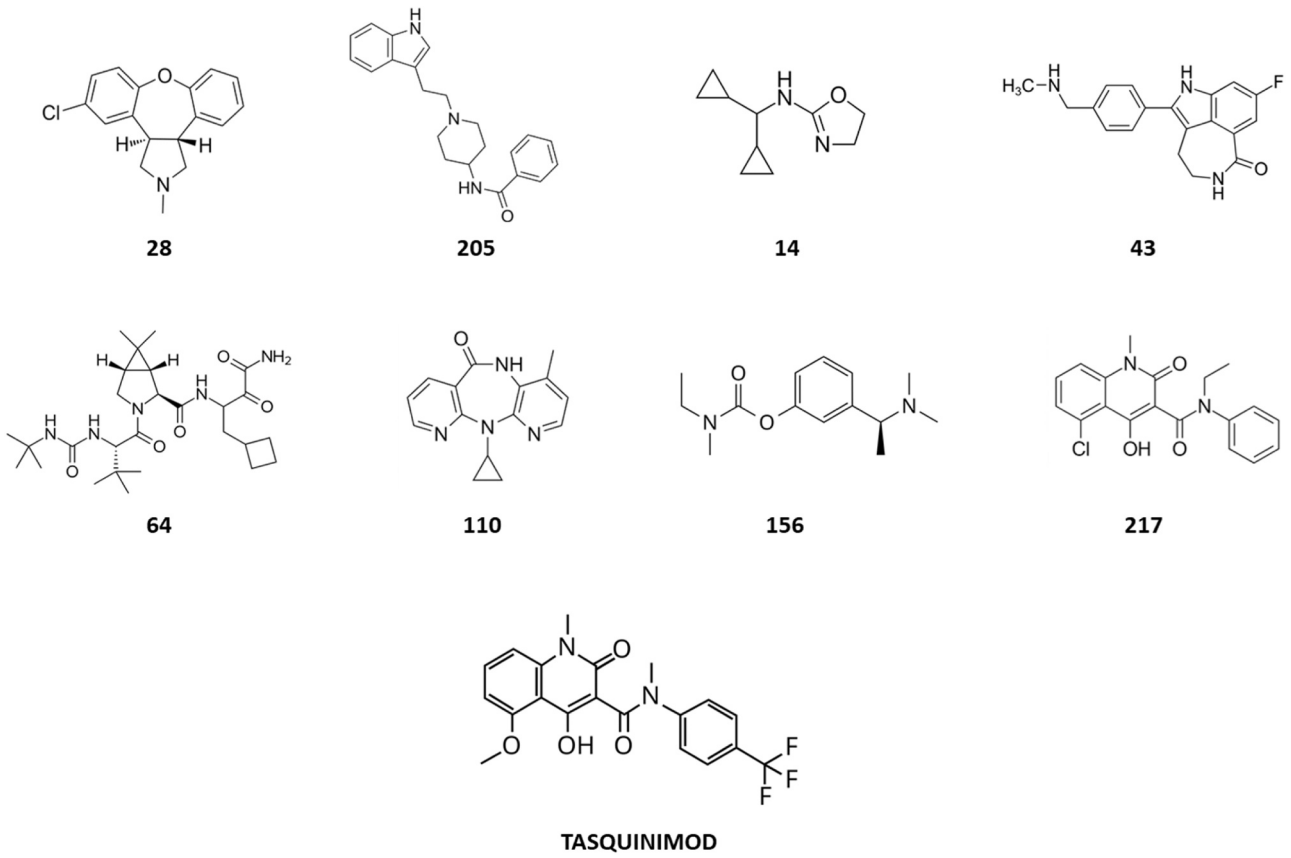

Fig. 1. Chemical structures of the compounds selected for modelling and SPR evaluation. From left to right and top to bottom: asenapine (ligand 28), indoramine (ligand 205), rilmenidine (ligand 14), rucaparib (ligand 43), boceprevir (ligand 64), nevirapine (ligand 110), rivastigmine (ligand 156), and the reference allosteric HDAC4 inhibitor tasquinimod. Structures are presented as identified by virtual screening and selected on the basis of docking scores and interaction profiles.

Table 1
Reference number of ligands from the EMA database and the number of times each ligand was ranked among the top 100 best-performing compounds across four scoring functions.

Ligand ID	Commercial name	No. of Occurrences
28	ASENAPINE	4
205	INDORAMINE	4
14	RILMENIDINE	3
43	RUCAPARIB	3
64	BOCEPREVIR	3
110	NEVIRAPINE	3
156	RIVASTIGMINE	3
217	LAQUINIMOD	3

stabilizing interactions with PHE168 and PRO156, both located near the zinc ion. The ligand orientation supports π–π stacking and hydrophobic contacts within a confined region, indicating a high degree of geometric complementarity with the binding site. In contrast, tasquinimod, as reported in Fig. 3, a bulkier and more extended molecule, exhibits a more superficial binding pose, engaging in polar interactions with HIS198, GLY330, and GLY331, and a π–π interaction with PHE227. Notably, PHE168, which is key in the binding of asenapine, remains unengaged in the tasquinimod complex, suggesting suboptimal cavity occupation. The distinct binding topologies correlate with docking results, where asenapine consistently yielded a more favourable binding score than tasquinimod, supporting the notion of a stronger and more stable interaction. These findings suggest that asenapine may act as a more efficient HDAC4 binder, potentially due to its ability to exploit a narrower and deeper sub-pocket that tasquinimod fails to fully engage, despite its greater molecular complexity. This selective engagement may underlie a more potent or specific inhibitory effect on HDAC4 activity.

This correct binding orientation, combined with scoring consensus and favourable energetics, justified the selection of asenapine for downstream SPR validation and competition experiments against tasquinimod.

Of particular interest is tasquinimod, an investigational drug for the treatment of solid tumors. This compound is known as a selective allosteric inhibitor of HDAC4. Its binding prevents the formation of the HDAC4/N-CoR/HDAC3 complex, which is essential for histone deacetylation and the transcriptional regulation of various transcription factors, including those involved in tumor cell survival and proliferation [22]. A docking analysis of tasquinimod with HDAC4 was performed at the active site, and the resulting interaction map confirmed the formation of a complex within the binding pocket, consistent with the behaviour of other studied ligands. Moreover, the predicted binding energy was low, comparable to that of the top-ranked ligands identified in this study.

3.2. SPR analysis of the interaction of asenapine and tasquinimod with HDAC4

To evaluate the binding interactions between HDAC4 and the known allosteric inhibitor tasquinimod, as well as the repositioned compound asenapine, SPR experiments were performed. SPR monitors, in real time and under label-free conditions, the reversible interaction of soluble analytes with ligands immobilised on a sensor chip surface, through non-covalent supramolecular forces [32].

The enzyme immobilization step plays a pivotal role in determining the quality and interpretability of SPR interaction data. In this study, we employed an amine coupling strategy, one of the most widely used

Table 2
Amino acid residues involved in the binding between HDAC4 and each ligand (listed in the top row). Residues shared by multiple ligands are highlighted in red and blue.

28	205	14	43	64	110	156	217	TASQUINIMOD
	LEU 105							
			ASP 113					
	SER 114		SER 114					
			ASP 115					
			ASN 119					
		Zinc ion 141			**Zinc ion 141**	**Zinc ion 141**	**Zinc ion 141**	**Zinc ion 141**
PRO 156					**PRO 156**	**PRO 156**	**PRO 156**	
		HIS 158						
					GLY 167			
PHE 168		**PHE 168**		**PHE 168**	**PHE 168**	**PHE 168**	**PHE 168**	**PHE 168**
						CYS 169	CYS 169	
							ASP 196	
				HIS 198	HIS 198		HIS 198	HIS 198
				ASN 225				
						PHE 226		
				PHE 227	**PHE 227**	**PHE 227**	**PHE 227**	**PHE 227**
		ASP 290						
				PRO 298		PRO 298		
		LEU 299		**LEU 299**	**LEU 299**	**LEU 299**	**LEU 299**	
								GLY 330
					GLY 331			GLY 331
HIS 332		HIS 332						

immobilization methods owing to its flexibility, ease of use, high efficiency, and robustness. Its key advantage is the randomized orientation of the ligand, obtained by exploiting free amine groups. This condition closely mimics the native interaction environment of enzyme–ligand complexes in solution [33,34]. The random orientation is usually guaranteed by free and solvent-exposed amino groups of lysine, which are typically protonated under the pH conditions of the buffer solution used for the immobilization procedure [31]. In this way, all molecular surfaces remain equally accessible for the interaction with the analyte. Consequently, the measured kinetic and thermodynamic constants reflect the full range of possible orientations for both the immobilized ligand and the analyte. The amount of immobilised enzyme is particularly critical in small molecule interaction studies. One intrinsic limitation of SPR is its mass-dependence. The response signal is influenced by the molecular weight ratio between analyte and immobilized ligand. In the case of low-molecular-weight compounds such as asenapine, this disparity can reduce signal amplitude when interacting with a large target like HDAC4. A sufficiently dense ligand immobilization is therefore required to counterbalance this effect. Accordingly, the theoretical SPR response is directly proportional to two main factors: the density of ligand molecules immobilized on the surface and the ratio between the molecular weight (MW) of the analyte and that of the ligand. As the MW difference increases, particularly when the ligand is substantially larger than the analyte, and thus the ratio decreases, the theoretical SPR response obtained during the interaction is reduced. This reduction makes the detection of such interactions more challenging. Since the MW ratio is fixed without altering the intrinsic properties of the molecules, the only parameter that can be optimized to enhance the response is the density of immobilized ligand on the sensor surface.

To address this, a MAR sensor chip was selected. Compared to the conventional CDL, it provides an enhanced binding capacity due to a higher number of reactive COOH groups, which allows the immobilization of a greater number of ligand molecules at equivalent dextran surface coverage. The combination of amine coupling with the high ligand density of the MAR sensor enabled real-time monitoring of the HDAC4–asenapine interaction, closely simulating the native biomolecular process and overcoming the intrinsic limitations of the instrument. In parallel, the use of a VIVASPIN device enabled both buffer exchange

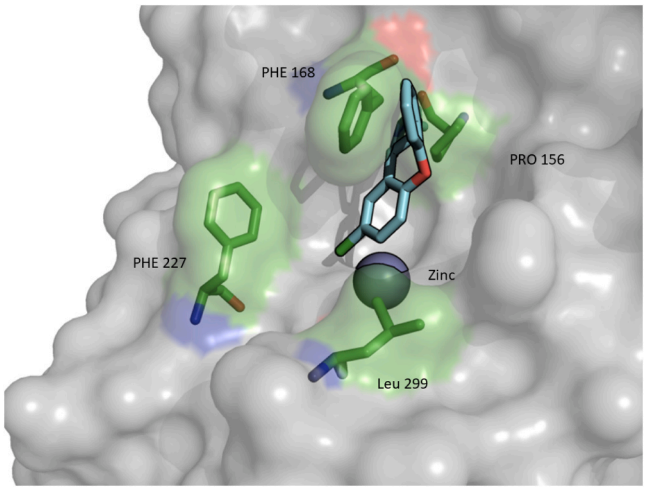

Fig. 2. The surface representation of HDAC4 shows the catalytic cavity with surrounding residues depicted as green sticks. The small molecule asenapine (cyan) is bound near the catalytic zinc ion (grey sphere). Notably, it engages in direct interactions primarily with residues PHE168 and PRO156, located deep in the binding pocket. In contrast, PHE227 and LEU299, although spatially close, do not appear to form direct contacts, possibly due to the small size and limited contact surface of asenapine.

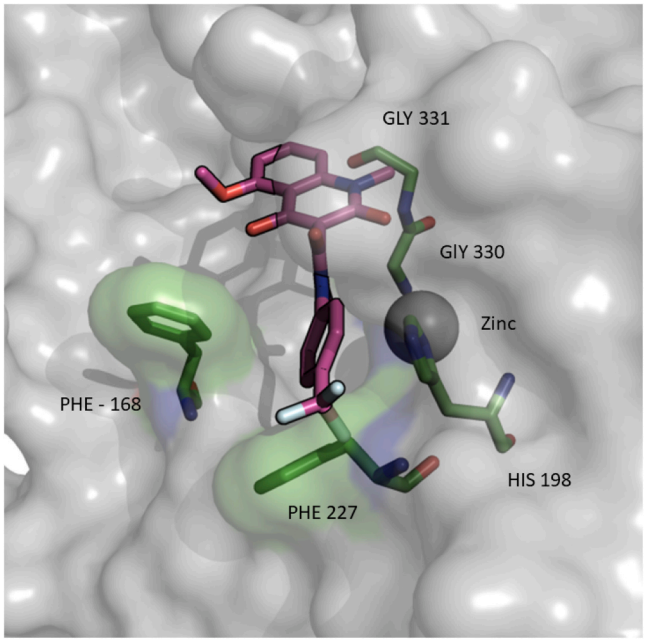

Fig. 3. Surface representation of HDAC4 showing the binding pocket occupied by tasquinimod (magenta), coordinated in close proximity to the catalytic zinc ion (dark grey sphere). The ligand forms polar interactions with HIS198, GLY330, and GLY331, while establishing a π–π stacking interaction with PHE227. The aromatic side chain of PHE168 is positioned nearby but does not engage in direct binding. The coordination with the zinc ion and interactions with surrounding residues suggest a stabilizing binding pose, consistent with the proposed inhibitory effect of tasquinimod on HDAC4 activity.

and preconcentration of the HDAC4 solution to the appropriate pH for efficient amine coupling. This methodological combination proved critical in achieving a high-density immobilization, thereby maximizing SPR sensitivity. This, in turn, enabled reliable kinetic analyses for small-molecule binding.

Injection of increasing concentrations of asenapine over the HDAC4-immobilized surface yielded progressively enhanced SPR responses (RU), consistent with concentration-dependent binding (Fig. 4A). The sensorgrams, doubly referenced by blank and reference channel subtraction, were analysed to extract kinetic and equilibrium parameters. The resulting equilibrium dissociation constant (K_D), calculated as the average of kinetic and steady-state determinations (dose-response plot), was 1.09 ± 0.02 μM.

The K_D value represents the ligand concentration at which half of the target sites are occupied [31,33], thus providing a quantitative measure of binding affinity: the lower the K_D, the higher the affinity [15,18,34]. Therefore, the low K_D value obtained for asenapine supports a high-affinity interaction with HDAC4.

The kinetic model employed assumes a 1:1 analyte-enzyme interaction. However, HDAC4 is a structurally dynamic, allosteric enzyme [22,35], and such a simplification may not consider relevant conformational changes. The adopted model, based on Sartorius technical documentation, accounts for a sequential interaction process:

$$E + A \rightleftharpoons EA \rightleftharpoons EA^*$$

where EA^* denotes the conformationally reorganized complex. Two assumptions support this model: *(i)* the conformational change occurs exclusively within the complex and not in the free enzyme; *(ii)* the reorganized complex EA* must revert to EA before dissociation.

From this, four kinetic constants are obtained: k_a ($M^{-1}s^{-1}$) and k_d (s^{-1}) describe the initial binding and dissociation events, while k_{a2} and k_{d2} refer to the forward and reverse conformational transitions, respectively. The K_D value thus integrates both the kinetic and conformational dynamics of the interaction, offering a mechanistically informed measure of binding affinity.

Concurrently, dose-response (Fig. 4B) curves were constructed by plotting equilibrium SPR responses (R_{eq}) against analyte concentration, yielding an independent estimation of K_D. The curves (Fig. 4A) exhibit a plateau between 100 and 180 s, corresponding to the equilibrium phase of asenapine binding. The steady-state K_D reflects the thermodynamic component of binding and is consistent with the calculated ΔG binding (Table 3), thereby corroborating the predicted stability of the HDAC4/asenapine complex.

To contextualize the binding behaviour of asenapine, tasquinimod, an established allosteric modulator of HDAC4 [22], was assessed under identical SPR conditions and served as a pharmacological benchmark. As shown in Fig. 5, the tasquinimod –HDAC4 follows a 1:1 binding model, yielding an equilibrium dissociation constant (K_D) of 8.05 ± 0.56 μM, calculated as the average of kinetic and steady-state determinations.

In comparison, asenapine exhibited a significantly lower K_D value (1.09 ± 0.02 μM), indicating a markedly higher affinity for HDAC4. This result aligns with the ΔG binding values obtained from computational modelling, where tasquinimod displayed a less favourable (less negative) free energy of binding relative to asenapine, corroborating its lower affinity at the molecular level.

Table 4 reports kinetic and affinity binding parameters derived from SPR analyses of HDAC4 interactions with tasquinimod and asenapine under distinct experimental conditions. The kinetic dissociation constant (K_D kinetic) was determined by fitting sensorgram data to the two-state conformational model previously described, incorporating both primary binding (k_{a1}, k_{d1}) and subsequent conformational transition (k_{a2}, k_{d2}) rate constants. Conversely, the affinity-based dissociation constant (K_D affinity) was extrapolated from the steady-state region of each sensorgram via dose–response analysis, wherein equilibrium SPR signals (R_{eq}) were plotted as a function of analyte concentration. These values were automatically computed using the instrument integrated evaluation software. The reported K_D average corresponds to the arithmetic mean of kinetic and affinity constants obtained from triplicate analyses for each condition.

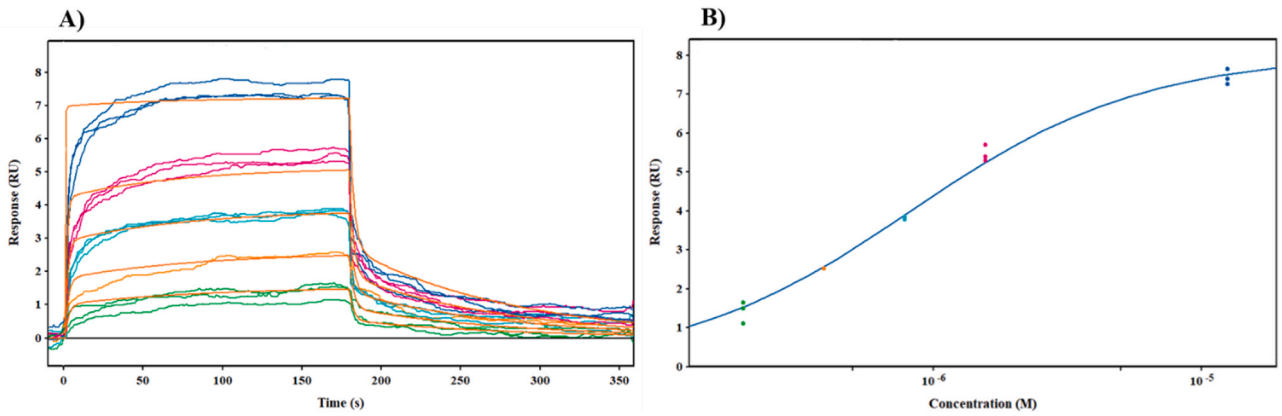

Fig. 4. A) Sensorgram of the interaction between varying asenapine concentrations (12.5 μM, 1.56 μM, 791 nM, 391 nM, 195 nM) and immobilised HDAC4 on the MAR sensor chip, showing increasing SPR response (RU) with rising analyte concentrations. Data were fitted to a 1:1 two-state binding model (red lines). **B)** Dose–response plot: equilibrium SPR responses (RU) at the sensorgram plateau (150–180 s) were plotted against asenapine concentration.

Table 3
Binding free energy (ΔG binding) calculated using Flare™ v.10.0.1 [24–26] software, considering the best docking pose for each ligand.

LIGANDS	MM/GBSA dG
14	−220,98
156	−207,91
43	−201,71
64	−201,1
28	−200,97
205	−195,74
110	−191,05
TASQUINIMOD	−186,12
217	−180,42

3.3. Competitive assay

To determine whether tasquinimod modulates or interferes with the binding of asenapine to HDAC4, a competition assay was conducted. Immobilised HDAC4 was exposed to asenapine solutions pre-incubated with fixed concentrations of tasquinimod (500 nM and 5 μM), while the asenapine concentration was gradually increased.

Although tasquinimod and asenapine are predicted to interact with distinct regions of HDAC4, the presence of tasquinimod may nonetheless induce conformational changes that affect asenapine binding. This experimental configuration was therefore designed to probe potential indirect or allosteric interference, rather than direct site competition.

The kinetic data were interpreted using the same two-state conformational model previously applied to the individual ligand analyses, allowing for consistent comparison across experimental conditions.

The K_D values obtained, 2.27 ± 0.19 μM and 6.38 ± 0.18 μM for the experiments conducted in the presence of 500 nM and 5 μM tasquinimod, respectively, demonstrate a progressive reduction in binding affinity as the concentration of tasquinimod increases.

In the absence of tasquinimod, asenapine binds HDAC4 with a K_D of 1.09 μM, indicating a high affinity for the enzyme, significantly greater than that observed for tasquinimod alone. However, when 500 nM tasquinimod was added to the asenapine solutions (Figure S2 A, B), the affinity for HDAC4 decreased, with a K_D of 2.27 μM. A further reduction in affinity was observed upon addition of 5 μM tasquinimod (Figure S2 C, D), resulting in a K_D of 6.37 μM. These results suggest that tasquinimod interferes with the binding of asenapine to HDAC4 in a concentration-dependent manner. The progressive increase in K_D is consistent with a competitive inhibition model, suggesting that tasquinimod may compete with asenapine for the same or a partially overlapping binding site on HDAC4, or alternatively exert an allosteric effect

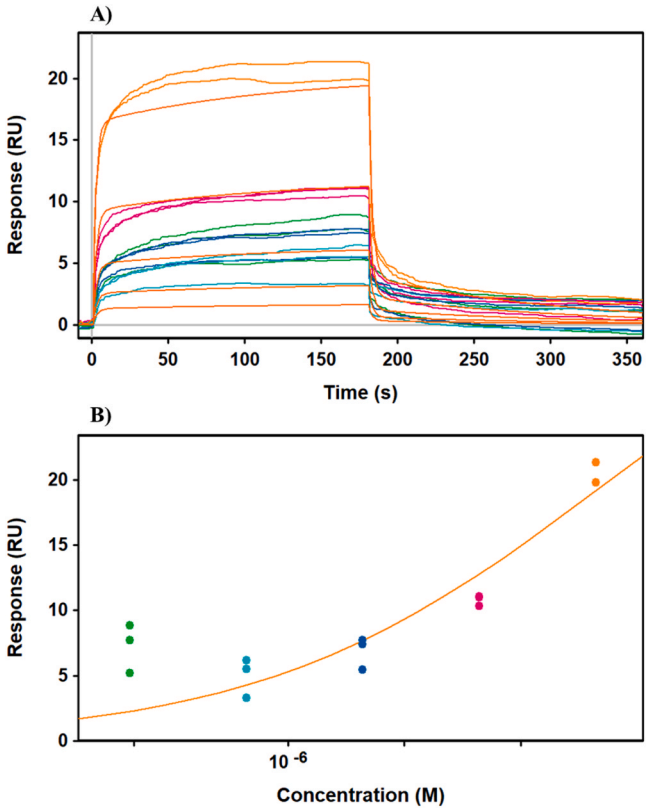

Fig. 5. A) Sensorgram of the interaction between varying tasquinimod concentrations (6.25 μM, 3.13 μM, 1.56 μM, 781 nM, and 391 nM) and immobilized HDAC4 on the MAR sensor chip, showing increasing SPR response (RU) with rising analyte concentrations. Data were fitted to a 1:1 two-state binding model (red lines). **B)** Dose–response plot: equilibrium SPR responses (RU) at the sensorgram plateau (150–180 s) were plotted against tasquinimod concentration.

that diminishes the binding affinity towards asenapine. In the case of competitive binding, the SPR signal obtained for the ligand mixture lies at an intermediate value between the individual responses elicited by asenapine and tasquinimod alone. Correspondingly, the K_D derived under these conditions fall within the range delimited by the K_D values of the individual ligands, further supporting a competitive or partially overlapping interaction scenario [36].

Detailed kinetic parameters, including association and dissociation

Table 4
Kinetic parameters derived from SPR interaction analyses between HDAC4 and tasquinimod, asenapine, and their combinations in competitive binding assays. Association (k_{a_1}, k_{a_2}) and dissociation (k_{d_1}, k_{d_2}) rate constants were extracted using a two-state model. Equilibrium dissociation constants (K_D) are reported as the mean ± SD from triplicate experiments from K_D (kinetic) and K_D (affinity). Reduced χ^2 values indicate the goodness of fit for each kinetic model.

Sample	$k_{a1}(M^{-1}s^{-1})$	$k_{a2}(s^{-1})$	$k_{d1}(s^{-1})$	$k_{d2}(s^{-1})$	K_D (M) (Kinetic)	K_D (M) (Affinity)	K_D(M) (Average)	Chi^2
Tasquinimod	$2.95 \pm 0.06e^4$	$2.86 \pm 0.07e^{-3}$	0.36 ± 0.04	$6.9 \pm 0.2e^{-3}$	9.02 ± 0.43 µM	7.1 ± 0.7 µM	**8.05 ± 0.56 µM**	1.86
Asenapine	$4.86 \pm 0.03e^4$	$8.91 \pm 0.07e^{-3}$	6.68 ± 0.04	$1.5 \pm 0.1e^{-3}$	1.37 ± 0.02 µM	810 nM±20	**1.09 ± 0.02 µM**	0.80
Competitive assay								
Asenapine + 500 nM tasquinimod	$9.3 \pm 0.5e^4$	$1.6 \pm 0.2e^{-3}$	0.25 ± 0.01	$5.4 \pm 0.7e^{-3}$	2.74 ± 0.07 µM	1.8 ± 0.3 µM	**2.27 ± 0.19 µM**	0.55
Asenapine + 5 µM tasquinimod	$9.7 \pm 0.2e^4$	$1.33 \pm 0.08e^{-3}$	0.64 ± 0.02	$8.0 \pm 0.4e^{-3}$	6.66 ± 0.06 µM	6.1 ± 0.3 µM	**6.38 ± 0.18 µM**	0.33

rate constants, are reported in Table 4.

4. Conclusions

A–T remains a debilitating neurodegenerative disorder with no curative therapies currently available. The aberrant nuclear accumulation of HDAC4 observed in Purkinje neurons of ATM-deficient individuals has been implicated in histone hypoacetylation and neuronal apoptosis, underscoring the relevance of HDAC4 as a therapeutic target.

In this study, we employed an integrative pipeline combining *in silico* drug repositioning and SPR to identify and characterise small-molecule HDAC4 modulators. The antipsychotic drug asenapine emerged as a promising candidate, exhibiting favourable docking scores and a low predicted binding free energy. Subsequent SPR analysis confirmed its high binding affinity for immobilised HDAC4, yielding a K_D of 1.09 µM. Competition assays demonstrated that asenapine binding affinity to immobilised HDAC4 decreased in a concentration-dependent manner in the presence of tasquinimod, a known HDAC4 modulator.

This approach provides a direct and cost-effective framework for evaluating EMA-approved compounds, eliminating the need for de novo synthesis and avoiding the significant expenses commonly incurred in early-stage drug development.

Taken together, our results highlight the potential of repositioned agents such as asenapine to modulate HDAC4 function and offer a rational basis for further translational efforts targeting epigenetic dysregulation in A–T.

Funding

Italian Ministry of Health, Piano di Sviluppo e Coesione del Ministero della Salute 2014-2020 Pharma-HUB—Hub per il riposizionamento di farmaci nelle malattie rare del sistema nervoso in età pediatrica (CUP E63C22001680001—ID T4-AN-04)

CRediT authorship contribution statement

Giuseppe Grasso: Writing – review & editing, Writing – original draft, Visualization, Supervision, Resources, Project administration, Methodology, Funding acquisition, Formal analysis, Data curation, Conceptualization. **Alessia Distefano:** Writing – original draft, Validation, Investigation, Formal analysis, Data curation. **Matteo Pappalardo:** Writing – original draft, Methodology, Investigation, Formal analysis, Data curation. **Roberta Turco:** Methodology, Investigation, Data curation. **Salvatore Guccione:** Writing – review & editing, Writing – original draft, Supervision, Software, Resources, Project administration, Investigation, Funding acquisition, Formal analysis, Data curation, Conceptualization.

Declaration of Competing Interest

The authors declare that they have no known competing financial interests or personal relationships that could have appeared to influence the work reported in this paper.

Acknowledgments

This work was supported by the Italian Ministry of Health, Piano di Sviluppo e Coesione del Ministero della Salute 2014–2020, Project: Pharma-HUB—Hub per il riposizionamento di farmaci nelle malattie rare del sistema nervoso in età pediatrica (CUP E63C22001680001—ID T4-AN-04).

Appendix A. Supporting information

Supplementary data associated with this article can be found in the online version at doi:10.1016/j.biopha.2025.118621.

Data availability

Data will be made available on request.

References

[1] C. Rothblum-Oviatt, J. Wright, M.A. Lefton-Greif, S.A. McGrath-Morrow, T. O. Crawford, H.M. Lederman, Ataxia telangiectasia: a review, Orphanet. J. Rare Dis. 11 (1) (2016 Dec) 159.
[2] J. Li, J. Chen, C.L. Ricupero, R.P. Hart, M.S. Schwartz, A. Kusnecov, et al., Nuclear accumulation of HDAC4 in ATM deficiency promotes neurodegeneration in ataxia telangiectasia, Nat. Med 18 (5) (2012 May) 783–790.
[3] M.F. Lavin, Ataxia-telangiectasia: from a rare disorder to a paradigm for cell signalling and cancer, Nat. Rev. Mol. Cell Biol. 9 (10) (2008 Oct) 759–769.
[4] Y. Shiloh, Y. Ziv, The ATM protein kinase: regulating the cellular response to genotoxic stress, and more, Nat. Rev. Mol. Cell Biol. 14 (4) (2013 Apr) 197–210.
[5] E. Verdin, F. Dequiedt, H.G. Kasler, Class II histone deacetylases: versatile regulators, Trends Genet 19 (5) (2003 May 1) 286–293.
[6] Unraveling the hidden catalytic activity of vertebrate class IIa histone deacetylases | PNAS [Internet]. [cited 2025 Aug 3]. Available from: ⟨https://www.pnas.org/doi/abs/10.1073/pnas.0706487104⟩.
[7] Structural and Functional Analysis of the Human HDAC4 Catalytic Domain Reveals a Regulatory Structural Zinc-binding Domain - ScienceDirect [Internet]. [cited 2025 Aug 3]. Available from: ⟨https://www.sciencedirect.com/science/article/pii/S0021925820524125⟩.
[8] P. a Marks, W.S. Xu, Histone deacetylase inhibitors: potential in cancer therapy, J. Cell Biochem 107 (4) (2009) 600–608.
[9] HDAC4: Mechanism of Regulation and Biological Functions: Epigenomics: Vol 6, No 1 [Internet]. [cited 2025 Aug 3]. Available from: ⟨https://www.tandfonline.com/doi/abs/10.2217/epi.13.73⟩.
[10] Drug repositioning: identifying and developing new uses for existing drugs | Nature Reviews Drug Discovery [Internet]. [cited 2025 Aug 3]. Available from: ⟨https://www.nature.com/articles/nrd1468⟩.
[11] N. Nosengo, Can you teach old drugs new tricks? Nature 534 (7607) (2016 Jun 1) 314–316.
[12] Orphan designation: Overview | European Medicines Agency (EMA) [Internet]. 2009 [cited 2025 Aug 3]. Available from: ⟨https://www.ema.europa.eu/en/human-regulatory-overview/orphan-designation-overview⟩.
[13] O.K.F. Ma, S. Ronsisvalle, L. Basile, A.W. Xiang, C. Tomasella, F. Sipala, et al., Identification of a novel adiponectin receptor and opioid receptor dual acting agonist as a potential treatment for diabetic neuropathy, Biomed. Pharmacother. 158 (2023 Feb 1) 114141.
[14] G. Jeschke, DEER distance measurements on proteins, Annu Rev. Phys. Chem. 63 (1) (2012 May 5) 419–446.
[15] A. Distefano, G. Antonio Zingale, G. Grasso, An SPR-based method for hill coefficient measurements: the case of insulin-degrading enzyme, Anal. Bioanal. Chem. 414 (17) (2022 Jul 1) 4793–4802.
[16] G. Grasso, A.I. Bush, R. D'Agata, E. Rizzarelli, G. Spoto, Enzyme solid-state support assays: a surface plasmon resonance and mass spectrometry coupled study of immobilized insulin degrading enzyme, Eur. Biophys. J. 38 (4) (2009) 407–414.
[17] G.A. Zingale, A. Distefano, G. Grasso, The use of surface plasmon resonance to study the interactions of proteins involved in conformational diseases:

experimental approaches for new therapeutical perspectives, Curr. Med Chem. 30 (36) (2023 Nov 1) 4072–4095.
[18] M.A. Cooper, Optical biosensors in drug discovery, Nat. Rev. Drug Discov. 1 (7) (2002 Jul) 515–528.
[19] H.Y. Meltzer, A. Dritselis, U. Yasothan, P. Kirkpatrick, Asenapine, Nat. Rev. Drug Discov. 8 (11) (2009 Nov 1) 843–844.
[20] O. Ursu, J. Holmes, J. Knockel, C.G. Bologa, J.J. Yang, S.L. Mathias, et al., DrugCentral: online drug compendium, Nucleic Acids Res 45 (D1) (2017 Jan 4) D932–D939.
[21] D.S. Kalinowski, D.R. Richardson, The evolution of iron chelators for the treatment of iron overload disease and cancer, Pharmacol. Rev. 57 (4) (2005 Dec 1) 547–583.
[22] J.T. Isaacs, L. Antony, S.L. Dalrymple, W.N. Brennen, S. Gerber, H. Hammers, et al., Tasquinimod is an allosteric modulator of HDAC4 survival signaling within the compromised cancer microenvironment, Cancer Res 73 (4) (2013 Feb 14) 1386–1399.
[23] A. Acharya, M. Yadav, M. Nagpure, S. Kumaresan, S.K. Guchhait, Molecular medicinal insights into scaffold hopping-based drug discovery success, Drug Discov. Today 29 (1) (2024 Jan 1) 103845.
[24] T. Cheeseright, M. Mackey, S. Rose, A. Vinter, Molecular field extrema as descriptors of biological activity: definition and validation, J. Chem. Inf. Model 46 (2) (2006 Mar 1) 665–676.
[25] M.R. Bauer, M.D. Mackey, Electrostatic complementarity as a fast and effective tool to optimize binding and selectivity of Protein–Ligand complexes, J. Med Chem. 62 (6) (2019 Mar 28) 3036–3050.
[26] M. Kuhn, S. Firth-Clark, P. Tosco, A.S.J.S. Mey, M. Mackey, J. Michel, Assessment of binding affinity via alchemical Free-Energy calculations, J. Chem. Inf. Model 60 (6) (2020 Jun 22) 3120–3130.
[27] G. Jones, P. Willett, R.C. Glen, A.R. Leach, R. Taylor, Development and validation of a genetic algorithm for flexible docking1, J. Mol. Biol. 267 (3) (1997 Apr 4) 727–748.
[28] H. Gohlke, D.A. Case, Converging free energy estimates: MM-PB(GB)SA studies on the protein–protein complex Ras–Raf, J. Comput. Chem. 25 (2) (2004) 238–250.
[29] Biacore T.200 Getting Started.book [Internet]. [cited 2025 Aug 3]. Available from: https://instruments.iitb.ac.in/sites/default/files/sop/2024-12/BiacoreT200_gettingstarted_handbook_IITB%20SPR%20Central%20Facility.pdf.
[30] HDAC4 – BioEntity: BE0003523 [Internet]. Available from: https://go.drugbank.com/bio_entities/BE0003523.
[31] Schasfoort R.B.M. Handbook of Surface Plasmon Resonance: 2nd Edition. Royal Society of Chemistry; 2017. 555 p.
[32] G. Grasso, R. D'Agata, L. Zanoli, G. Spoto, Microfluidic networks for surface plasmon resonance imaging real-time kinetics experiments, Microchem J. 93 (1) (2009) 82–86.
[33] E.C. Hulme, M.A. Trevethick, Ligand binding assays at equilibrium: validation and interpretation, Br. J. Pharmacol. 161 (6) (2010) 1219–1237.
[34] J. Homola, Surface plasmon resonance sensors for detection of chemical and biological species, Chem. Rev. 108 (2) (2008 Feb 1) 462–493.
[35] H. Liu, F. Zhang, K. Wang, X. Tang, R. Wu, Conformational dynamics and allosteric effect modulated by the unique zinc-binding motif in class IIa HDACs, Phys. Chem. Chem. Phys. 21 (23) (2019) 12173–12183.
[36] W. Huber, F. Mueller, Biomolecular interaction analysis in drug discovery using surface plasmon resonance technology, Curr. Pharm. Des. 12 (31) (2006 Nov 1) 3999–4021.